Journal of Alloys and Compounds 863 (2021) 158081

Contents lists available at ScienceDirect

Journal of Alloys and Compounds

journal homepage: www.elsevier.com/locate/jalcom

# Hierarchical nanosheets of ternary CoNiFe layered double hydroxide for supercapacitors and oxygen evolution reaction

R.C. Rohit[a], Ajay D. Jagadale[a,*], Surendra K. Shinde[b,*], D.-Y. Kim[b], Vijay S. Kumbhar[c], Masaharu Nakayama[c]

[a] Center for Energy Storage and Conversion, School of Electrical and Electronics Engineering, SASTRA Deemed University, Thanjavur 613401, Tamil Nadu, India
[b] Department of Biological and Environmental Science, College of Life Science and Biotechnology, Dongguk University, 32 Dongguk-ro, Biomedical Campus, Ilsandong-gu, Siksa-dong, 10326 Goyang-si, Gyeonggi-do, South Korea
[c] Department of Applied Chemistry, Graduate School of Sciences and Technology for Innovation, Yamaguchi University, 2-16-1 Tokiwadai, Ube 755-8611, Japan

ARTICLE INFO

*Article history:*
Received 29 August 2020
Received in revised form 17 November 2020
Accepted 21 November 2020
Available online 25 November 2020

*Keywords:*
Layered double hydroxide
Electrodeposition
Supercapacitor
Electrocatalyst
Oxygen evolution reaction

ABSTRACT

The preparation of stable and efficient thin films with excellent energy storage and conversion capabilities has attracted great attention in the field of supercapacitors and electrocatalysis. Herein, hierarchical nanosheets-based ternary CoNiFe layered double hydroxide (LDH) thin films are prepared via an inexpensive and facile electrodeposition method. The structural, morphological, and electrochemical properties of films are systematically studied and compared with their binary counterparts. As prepared CoNiFe LDH shows a maximum specific capacity of 360 C $g^{-1}$ at the current density of 0.4 A $g^{-1}$ with a capacity retention of 51% even at the higher current density of 10 A $g^{-1}$. Moreover, it shows excellent cyclic stability of 84% after 2000 cycles. As an electrocatalyst, CoNiFe LDH demonstrates an excellent performance in OER, affording an overpotential of 196 mV at the current density of 10 mA $cm^{-2}$ with a Tafel slope value of 49 mV $dec^{-1}$. Also, it depicts excellent catalytic stability with stable operation for over 10 h. Thus, ternary CoNiFe LDH thin film can be used as a promising electrode material for both electrochemical energy storage and catalysis.



## 1. Introduction

The continuously increasing energy consumption and concerns over environmental pollution require significant global efforts on efficient generation, storage, and transmission of energy [1]. The electrochemical energy storage and electrocatalysis have been considered to be the most effective technologies to remove the aforementioned stumbling block [2]. Among electrochemical energy storage devices, such as batteries and supercapacitors (SCs), SCs have attracted great importance owing to their high specific capacitance, long cycle life, and high power density [3]. The SC bridges the gap between conventional capacitors and rechargeable batteries by combining advantages of both. However, SCs are characterized by their poor energy density. Therefore, a variety of different materials has been investigated to improve the energy density of SCs [4]. SCs are categorized into electric double layer capacitors (EDLCs) and pseudocapacitors. Compared with EDLCs, pseudocapacitors demonstrate superior capacitive performance owing to the involvement of fast redox reactions and tremendous scales of electrostatic charge diffusion and accumulation [5]. Electrode materials such as transition metal oxides, hydroxides, sulfides, carbides, nitrides, conducting polymers, etc. neither exhibit pure pseudocapacitive nor faradaic behavior. These materials can be classified as battery-like electrodes which have attracted great attention in recent years [6].

On the other hand, the electrochemical water splitting using high-performance electrocatalysts is imperative to produce oxygen and hydrogen for fuel cell and metal-air battery technologies [7]. During water splitting, the hydrogen evolution reaction (HER) is a straightforward process that readily happens at low overpotential. However, the oxygen evolution reaction (OER) ($4OH^- \rightarrow O_2 + 2H_2O + 4e^-$) is an arduous process owing to the sluggish four-electron transfer steps [2]. Previously, transition metal oxides such as $RuO_2$ and $IrO_2$ have been reported as high-performance electrocatalysts for OER [8]. However, it is important to explore highly competent and inexpensive OER catalysts based on earth-abundant elements.

Recently, transition metal-based layered double hydroxides (LDHs) have attracted great attention in the field of SCs, electrocatalysts, and electrochemical sensors because of their highly reversible redox kinetics, cost-effectiveness and excellent structural and compositional tunability [9–11]. The general formula for LDHs is

* Corresponding authors.
*E-mail addresses:* ajaydattujagadale@eee.sastra.edu (A.D. Jagadale), surendrashinde@dongguk.edu (S.K. Shinde).

https://doi.org/10.1016/j.jallcom.2020.158081
0925-8388/

$[M^{2+}_{1-x}M^{3+}_{x}(OH)_2]^{x+}[A^{n-}_{x/n}.mH_2O]^{x-}$ (where, $M^{2+}$ and $M^{3+}$ are the divalent and trivalent metal cations, respectively; $A^{n-}$ is the charge-balancing anion of valence n; $x = M^{3+} / (M^{2+} + M^{3+})$) [12]. Lately, the most popular LDHs like NiCo [13], CoAl [14], CoMn [12], NiAl [15], NiMn [16] have been reported as excellent electrode materials for electrochemical energy applications. Amongst all LDHs, much work has been reported on the synthesis of α-phase NiCo LDH for supercapacitor as well as electrochemical catalytic applications. The α-phase exhibits larger interlayer spacing compared to β-phase which gives superior electrochemical performance owing to the rapid ion transport in the electrode. However, after a few charging-discharging cycles, the α-phase transforms into the β-phase in the presence of KOH electrolyte which degrades the electrochemical performance over time [17]. This drawback can be overcome by partially substituting host metal ions by third trivalent metal ions, such as $Fe^{3+}$ or $Al^{3+}$ which form the ternary LDH. In particular, the addition of a third metal ion in the binary LDH can modify the electronic structure and enhance the electric conductivity, offering a huge number of active sites with a rapid electron transfer process [7,18]. The selection of $Fe^{3+}$ ion as a third cation is obvious because of the contribution of $Fe^{3+}/Fe^{2+}$ redox couple for the enhancement of electrochemical performance [17,19,20]. In earlier reports, CoNiFe ternary LDH has been prepared via complex and time-consuming methods for energy-related applications, limiting their practical applicability for large scale production [21–24].

Therefore, in the present work, Co, Ni, and Fe based ternary LDH thin films are prepared for the first time via rapid, inexpensive and facile electrodeposition method. The structural, morphological and electrochemical properties of the film are systematical studied and compared with their binary counterparts. As prepared CoNiFe LDH shows a maximum specific capacity of 360 C $g^{-1}$ at the current density of 0.4 A $g^{-1}$ with a capacity retention of 51% even at the higher current density of 10 A $g^{-1}$. Further, it shows excellent cyclic stability of 84% after 2000 cycles. Besides, as an electrocatalyst, the CoNiFe LDH demonstrates an excellent performance in OER, affording an overpotential of 196 mV at the current density of 10 mA $cm^{-2}$ and Tafel slope value of 49 mV $dec^{-1}$ with stable operation for over 10 hours.

## 2. Experimental section

### 2.1. Chemicals and materials

Analytical grade cobalt nitrate hexahydrate ($Co(NO_3)_2{\cdot}6H_2O$), nickel nitrate hexahydrate ($Ni(NO_3)_2{\cdot}6H_2O$), sodium nitrate ($NaNO_3$), and ferrous sulfate heptahydrate ($FeSO_4{\cdot}7H_2O$) were purchased from Sisco Research Laboratories Pvt. Ltd. (SRL), India and potassium hydroxide (KOH) pellets were purchased from Sigma-Aldrich, USA. The stainless steel (SS) of grade 304 with a thickness of 0.05 mm was purchased from Labtronics enterprises, India.

### 2.2. Synthesis of LDHs

The preparation of binary/ternary LDHs was achieved by electrodeposition using a three-electrode system. The stainless steel (SS) (exposed area 1 × 1 $cm^2$), Ag/AgCl (3 M NaCl) and coiled platinum were used as a working, reference and counter electrodes, respectively. Prior to deposition, SS electrodes (1 × 6 $cm^2$) were cleaned with deionized water and ethanol using an ultrasonicator. The electrodeposition bath for ternary CoNiFe LDH was prepared by mixing 0.1 M $Co(NO_3)_2{\cdot}6H_2O$, 0.1 M $Ni(NO_3)_2{\cdot}6H_2O$ and 0.1 M $FeSO_4{\cdot}7H_2O$ in the ratio of 1:1:1. To this solution, 0.1 M of $NaNO_3$ was added to increase the concentration of $OH^-$ ions, accelerating the rate of deposition which resulted into in high-quality uniform thin films. The electrolyte for binary LDHs such as CoNi, CoFe and NiFe was prepared by adding the corresponding nitrate sources to the deionized water in the ratio of 1:1. All the depositions were carried out at the cathodic current density of 1 mA $cm^{-2}$ for 5 min. Furthermore, deposited films were dried overnight at room temperature. Thin films such as CoNiFe LDH, CoNi LDH, CoFe LDH and NiFe LDH were labeled as CNFL, CNL, CFL and NFL, respectively. Finally, prepared samples were subjected to further elemental, morphological and electrochemical characterizations.

### 2.3. Materials characterization

X-ray diffraction (XRD) patterns were recorded using an X-ray diffractometer (Rigaku, Ultima IV) equipped with a Cu Kα radiation source (λ = 1.5406 Å). The compositional studies of the samples were examined using energy-dispersive X-ray spectrometry (EDS) (JSM6701f, JEOL, Japan), X-ray photoelectron spectroscopy (XPS) (ULVAC-PHI Quantera SXM), Fourier-transform infrared spectroscopy (Vertex 80v, Bruker) and Raman spectroscopy (XperRam 200). The morphology and microstructure of the sample were examined using FE-SEM (JEOL JSM-7100) and TEM (JSM2100, JEOL, Japan). The mass of the active material on the SS substrate was measured by the weight difference method using an electronic balance (CAI-35, Contech Instruments Ltd).

### 2.4. Electrochemical measurements and evaluation

The supercapacitive and electrocatalytic performances were evaluated using a three-electrode system via Biologic SP-150 electrochemical workstation. In the three-electrode system, thin films on the SS substrate, coiled platinum, and Ag/AgCl were used as a working, counter and reference electrodes, respectively. The freshly prepared solutions of 2 M and 1 M KOH were used as an electrolyte for supercapacitive and catalytic studies, respectively. The electrocatalytic activity of the electrode was examined using linear sweep voltammetry (LSV), cyclic voltammetry (CV), and chronoamperometry techniques. The specific capacity of the electrodes was calculated from the CV curves using following relation,

$$C = \frac{\int_{v_1}^{v_2} I(V)dv}{M\,s}\,C\,g^{-1} \quad (1)$$

where 'C' is the capacity (C $g^{-1}$), 'M' is the mass of the active material (g), 's' is the scan rate (V $s^{-1}$), and $\int_{v_1}^{v_2} I(V)dv$ is the area under the CV curve. The specific capacity was also calculated from the GCD curves using following relation,

$$C = \frac{I \times \Delta t}{M}\,C\,g^{-1} \quad (2)$$

where 'I′ is the discharging current (A), 'Δt' is the discharging time (s), and 'M' is the mass of the active material (g) [25,26]. Electrochemical impedance spectroscopy (EIS) was performed in the frequency range of 0.1 Hz to 1 MHz. Furthermore, values of overpotential were calculated using following formula,

$$\eta = E_{vs.RHE} - 1.23\ V = E_{vs.Ag/AgCl} - 0.221\ V \quad (3)$$

where 'η' is overpotential (mV), '$E_{vs.RHE}$' is the potential vs. RHE (reversible hydrogen electrode) (mV), '$E_{vs.Ag/AgCl}$' is the potential vs. Ag/AgCl reference electrode and '1.23 V' is standard thermodynamical potential for oxygen reduction.

## 3. Results and discussion

### 3.1. Preparation of LDHs

The deposition was based on the reduction reaction of nitrate and sulfate ions, leading to the increase of the pH near the surface of the substrate, accelerating the deposition process [27]. The formation of binary and ternary LDHs can be described using the following reactions [28] and Fig. 1.

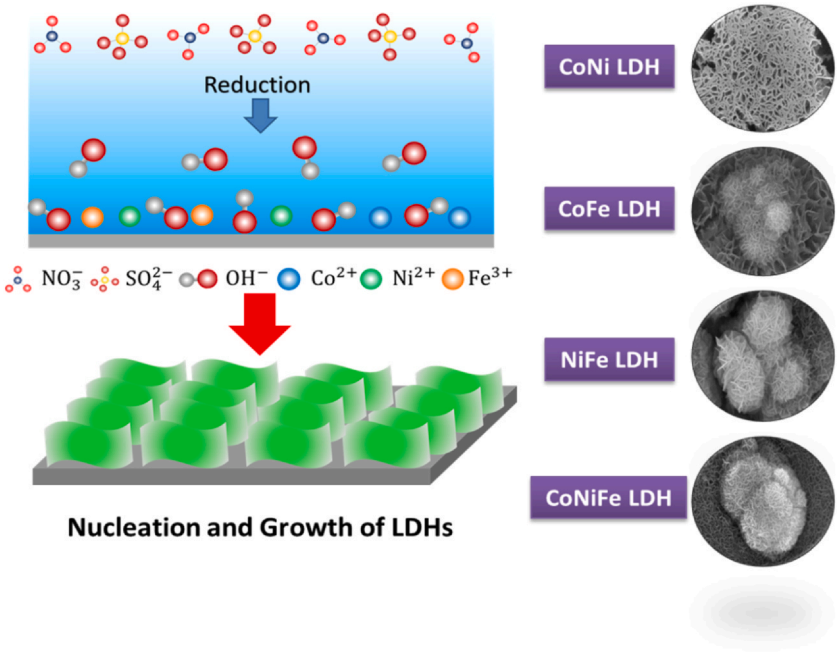


**Fig. 1.** Schematic of preparation of LDHs thin films.

$$NO_3^- + H_2O + 2e \rightarrow NO_2^- + 2OH^- \quad (4)$$

$$SO_4^{2-} + H_2O + 2e \rightarrow SO_3^{2-} + 2OH^- \quad (5)$$

$$M^{x+}(Co^{2+}, Ni^{2+}, Fe^{3+}) + xOH \rightarrow M(OH)_x \quad (6)$$

The schematic diagram shows the reduction process of nitrate and sulfate ions and subsequent precipitation of $Co^{2+}$, $Ni^{2+}$ and $Fe^{3+}$ ions forming LDHs.

### 3.2. Morphological study

The FESEM images of CNL, CFL, NFL and CNFL samples are shown in Fig. 2, demonstrating the formation of distinct microstructures. As shown in Fig. 2A, a CNL sample was formed with a network-like structure having densely packed nanosheets. The CFL sample exhibited the creation of interconnected nanoflakes which are agglomerated to form nanoflowers like morphology (Fig. 2B). Similarly, the FESEM image of the NFL sample presents the formation of nanoflakes which assembled to

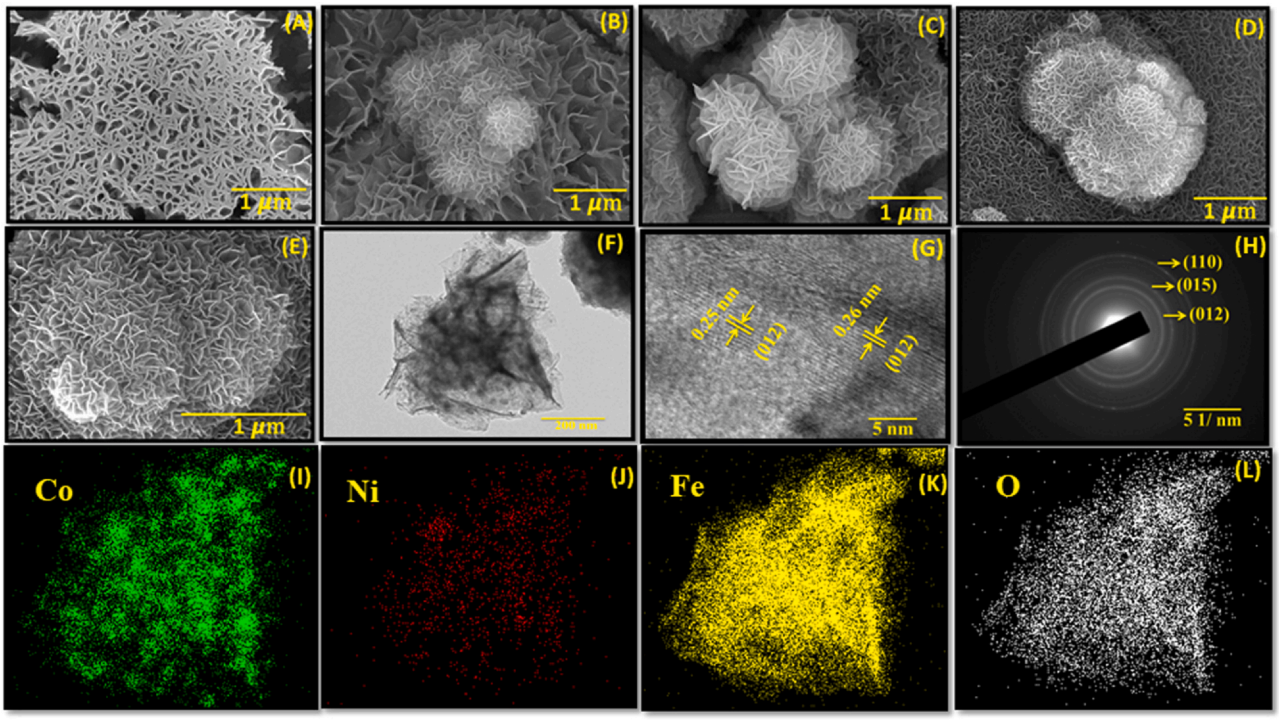


**Fig. 2.** FESEM images of (A) CNL, (B) CFL, (C) NFL, (D) CNFL samples at 30,000×, (E) CNFL at 50,000× magnification, (F) TEM image of CNFL, (G) HR-TEM image of CNFL, (H) SAED pattern and (I–L) elemental mapping of Co, Ni, Fe and O corresponding to TEM image.

form hierarchical spheres (Fig. 2C). As shown in Fig. 2D and E, the CNFL exhibits hierarchical nanosheets like structure. These internally connected nanosheets form a strong network which can be helpful in an electrochemical application. The average thicknesses of deposited nanostructures were evaluated from the FESEM images at the magnification of 50,000× (Fig. S1 and Table S1). The ternary CNFL sample depicted the average thickness of 32.8 nm which may lead to the higher surface area and more electrochemical active sites [29,30]. Therefore, as compared to other binary LDHs, the microstructure of a ternary CoNiFe LDH may facilitate high surface area and open channels, rewarding superior catalytic and electrochemical energy storage activities. The open and porous structure of CNFL electrode provide excellent pathways for hassle-free ionic and electronic transport [31]. Furthermore, Fig. 2F shows the TEM image of the CNFL sample, confirming the formation of nanosheets like microstructure. The high-resolution TEM (HR-TEM) image shows lattice fringes corresponding to the interplanar spacing of 0.25 and 0.26 nm that can be attributed to the (012) plane of CoNiFe LDH phase (Fig. 2G). The selected area electron diffraction (SAED) pattern (Fig. 2H) shows the diffraction concentric rings, verifying the polycrystalline nature of the CoNiFe LDH. These rings can be attributed to the (012), (015) and (110) crystal planes of CoNiFe LDH. Furthermore, elemental mapping images (Fig. 2I–L) show a uniform distribution of the Co, Ni, Fe and O in the ternary CoNIFe LDH nanosheets. Similar uniformity was obtained in case of mapping images taken from FESEM (Fig. S2).

### 3.3. Structural study

XRD patterns of thin films deposited on the SS substrate are shown in Fig. 3A. The peak at around 10° confirms the formation of LDH with a hydrotalcite-like structure. Peaks at around 10°, 19.5° and 59.8° corresponded to (003), (006) and (110) planes, respectively [21,32–34]. Two additional peaks at around 43.57° and 74.55° are attributed to the SS substrate material. The CNL sample shows two distinct peaks at 33.51° and 59.82° which are ascribed to the preferred growth along (012) and (110) directions, respectively [35]. The interplanar spacing in CNL, CFL, NFL and CNFL samples is calculated to be 9.2, 8.9, 10 and 9.5 Å, respectively. These values of interlayer spacing may sufficiently decrease the diffusion energy barrier for the ion intercalation and improve the interlayer conductivity [36].

Further, the elemental composition and chemical valence states on the surface of CNFL thin film were confirmed by XPS analysis as shown in Fig. 3(B–D). The survey spectrum confirms the presence of Co, Ni, Fe and O in the CNFL sample with atomic percentages of 6.91%, 3.89%, 4.78% and 49.66%, respectively (Fig. S3). The high-resolution spectrum of Co 2p (Fig. 3B) depicts two distinct peaks at 780.8 and 796.7 eV which are attributed to the Co $2p_{3/2}$ and Co $2p_{1/2}$ atomic orbitals, respectively, indicating the presence of $Co^{2+}$ and $Co^{3+}$ ions. The high spin state of the $Co^{2+}$ was highlighted by the two satellite peaks at 785.26 and 802.8 eV [26]. Fig. 3C represents the high-resolution spectrum of the Ni 2p, in which, $2p_{3/2}$ and $2p_{1/2}$ states were observed at 873.24 and 855.5 eV, respectively along with two satellite peaks at 861.3 and 879.6 eV [37]. The peaks at 711.3 and 724.7 eV (Fig. 3D) can be assigned to $2p_{3/2}$ and $2p_{1/2}$, respectively, indicating the existence of $Fe^{3+}$ in CoNiFe LDH [28]. This study confirmed the formation of CoNiFe LDH.

The FTIR spectrum (Fig. 3E) of CNFL also supported the formation of CoNiFe LDH with the strong band at 3284 $cm^{-1}$ corresponding to the stretching vibrations of the hydroxyl group [38]. The bending vibrations of $H_2O$ molecules present in interlayers appeared at 1634 $cm^{-1}$ [13]. The band at 1348 $cm^{-1}$ represents the stretching vibration of the $NO_3$ groups in the LDH interlayers [39]. The sharp peak at 1091 $cm^{-1}$ was attributed to the S–O stretching vibration in the sulfate ions [40]. The bands at around 400–800 $cm^{-1}$ are attributed to stretching vibrations of M–O and M–OH bonds (M = Co, Ni and Fe) [41]. As shown in the Raman spectrum (Fig. 3F) of the CNFL film, the characteristic peaks at 477 and 532 $cm^{-1}$

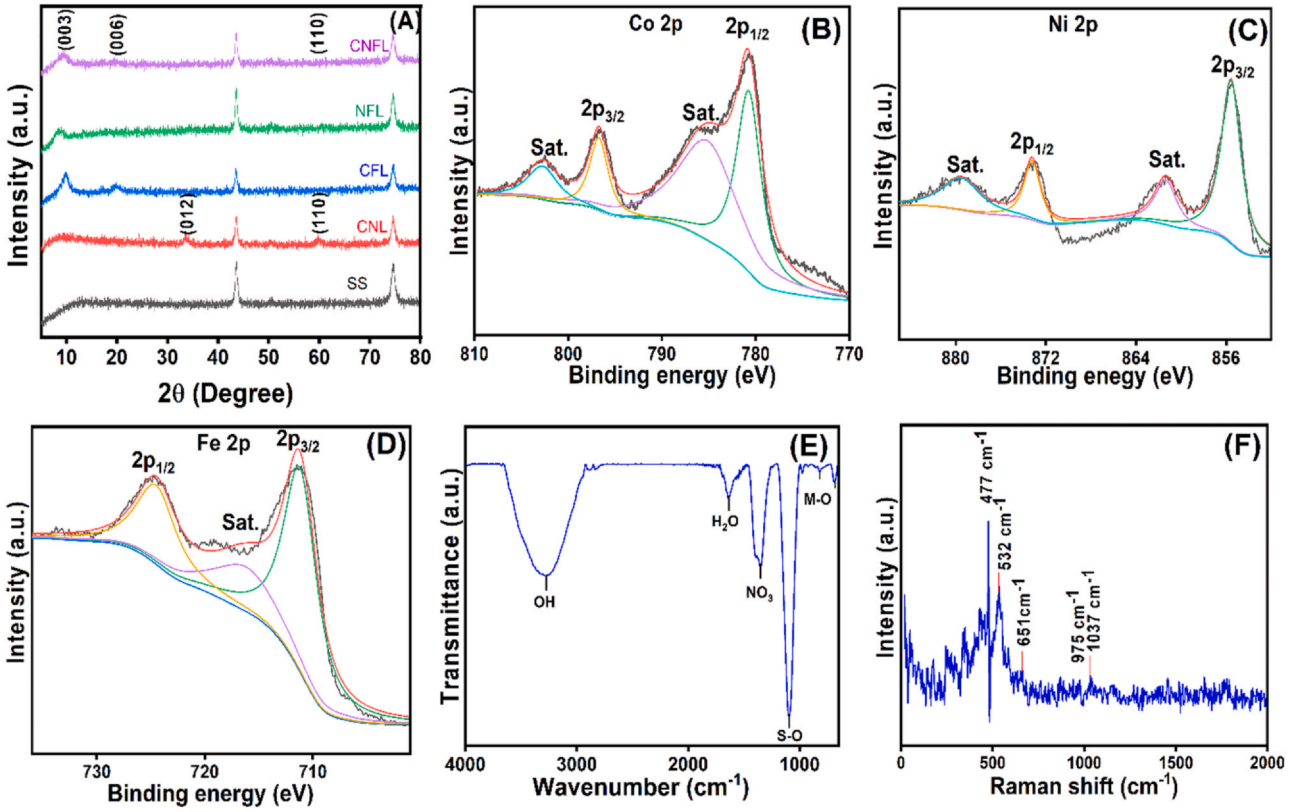


**Fig. 3.** (A) XRD patterns of SS, CNL, CFL, NFL and CNFL samples, high resolution spectrum of (B) Co 2p, (C) Ni 2p and (D) Fe 2p of CNFL thin film, (E) FTIR and (F) Raman spectra of CNFL sample.

are related to the M–O and M–OH bonds (where, M = Co, Ni, Fe) [42,43]. Peaks originated at 651 and 975 $cm^{-1}$ can be attributed to the sulfate ions in the interlayer spacing [44]. The presence of nitrate ions can be confirmed by the peak obtained at 1037 $cm^{-1}$ [45]. Therefore, the Raman spectrum supports the formation of CoNiFe LDH.

### 3.4. Supercapacitive study

The electrochemical performance of prepared electrodes was characterized using a three-electrode system via CV and GCD techniques. CV curves of CNL, CFL, NFL and CNFL film electrodes were presented at the scan rate of 5 mV $s^{-1}$ in Fig. 4A (CV curves at various scan rates can be seen in Fig. S4). Interestingly, all electrodes exhibited distinct redox peaks, confirming the faradaic battery-like behavior. As the scan rate was increased, oxidation and reduction peaks shifted towards more positive and negative potentials, respectively owing to the rapid redox reaction at the electrode-electrolyte interface [46]. Specific capacities of CNL, CFL, NFL and CNFL were calculated to be 53, 272, 8 and 338 C $g^{-1}$, respectively. It is seen that the ternary CoNiFe LDH exhibited excellent specific capacity as compared to other binary LDHs. It can be attributed to the enhanced electrical conductivity and electrochemically active sites created by the incorporation of a third transition metal cation [47]. Moreover, the interconnected nanosheets like microstructure of ternary CoNiFe LDH facilitates high surface area for efficient and rapid charge-discharge reactions at the electrode/electrolyte interface. Also, the open and porous structure provides hassle-free ionic and electronic diffusion through the electrode. Furthermore, the specific capacity of CNFL electrode was also calculated from the GCD curves. It was found as 360, 338, 326, 316, 268, 239, 215 and 187 C $g^{-1}$ at the current densities of 0.4, 0.6, 0.8, 1, 3, 5, 7 and 10 A $g^{-1}$, respectively (Fig. 4B). Specific capacities obtained from CV and GCD curves are in good agreement with each other. The maximum value of specific capacity in the present case is quite comparable with values reported in the literature for ternary and binary LDHs (Table 1). Generally, OER parasitism limits the charge storage performance of faradaic battery type electrodes and it must be suppressed as much as possible by shifting the onset potential towards a more positive side [58]. Although the OER parasitism in the ternary CoNiFe LDH was dominant, the charge storage performance was not compromised which may be attributed to the existence of high apparent surface area and the number of electrochemically active sites. Moreover, the CNFL electrode shows capacity retention of 51% even at the higher current density of 10 A $g^{-1}$ (Fig. S5D). It can be ascribed to the open and porous structure of the ternary CoNiFe LDH, providing easy and rapid pathways for electronic and ionic transport. Also, the cyclic stability of CNL, CFL, NFL and CNFL electrodes were examined at the current density of 10 A $g^{-1}$ for 2000 GCD cycles (Fig. 4C). Capacity retentions of 70%, 48%, 98% and 81% were obtained for CNL, CFL, NFL and CNFL electrodes, respectively. Although the NFL electrode exhibited excellent cyclic stability of 98%, the poor specific capacity hinders its practical application in supercapacitor. On the other hand, the ternary CoNiFe LDH displays excellent cyclic stability of 81.4% after 2000 cycles which is far better than other binary LDHs. The improved stability performance is attributed to the addition of the third cation in the ternary LDH.

Additionally, electrical parameters of electrodes were estimated by using the EIS (Fig. 4D). Nyquist plots of CNL, CFL, NFL and CNFL electrodes are shown in Fig. 3D, depicting a distinct semicircle at a higher frequency region. The equivalent circuit fitted for the impedance data consisted of bulk electrolyte resistance ($R_e$) and the charge transfer resistances ($R_{ct1}$ and $R_{ct2}$). The $R_{ct1}$ represents the charge transfer

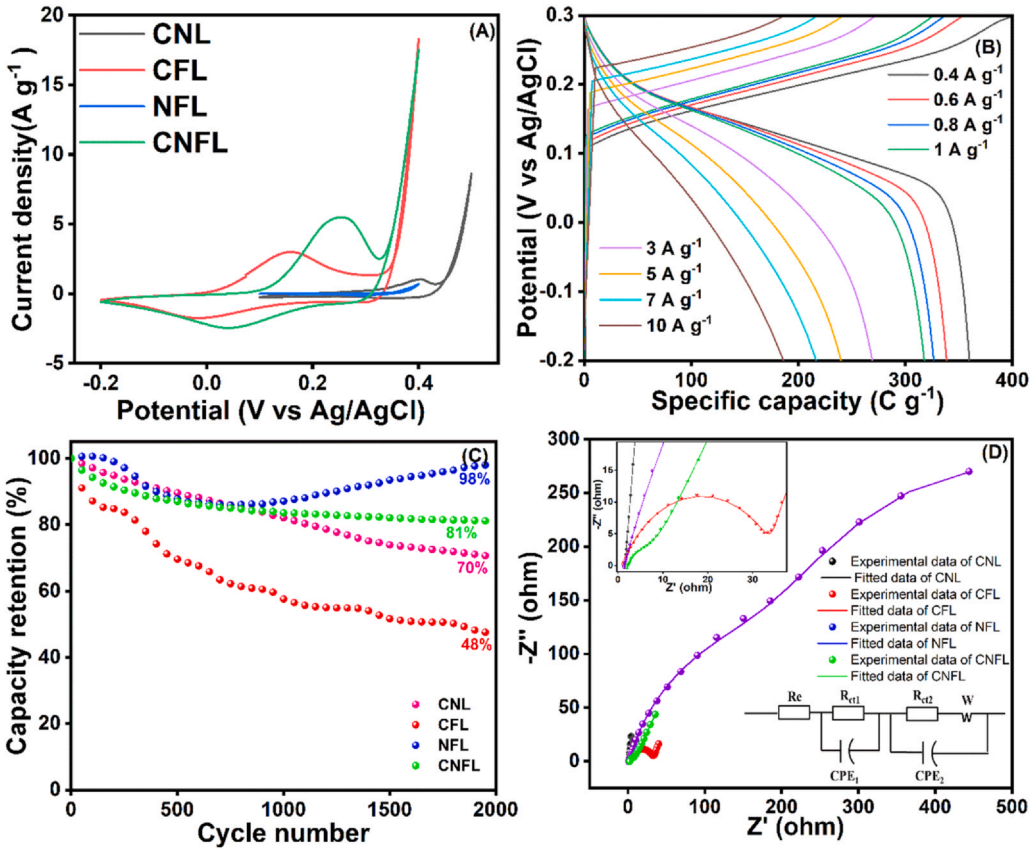


**Fig. 4.** (A) CV curves of CNL, CFL, NFL and CNFL electrodes at the scan rate of 5 mV $s^{-1}$, (B) GCD curves of CNFL electrode at different current densities, (C) the variation of capacity retention and cycle number and (D) Nyquist plots of CNL, CFL, NFL and CNFL electrodes (top inset: magnified higher frequency region and bottom inset: equivalent circuit diagram).

**Table 1**
Comparison of specific capacity of CoNiFe LDH with reported values.

| S.No | Material | Potential window (V vs Ag/AgCl) | Specific capacity ($C\,g^{-1}$) | Reference |
|---|---|---|---|---|
| 1 | CoNiFe LDH/CNFs | 0–0.6 | 721.8 | [21] |
| 2 | FeCoNi LDH | 0–0.55 | 539 | [24] |
| 3 | NiCoFe $(OH)_2$/polyaniline | −0.4–0.8 | 860.4 | [35] |
| 4 | Graphene/NiAl LDH | 0–0.6 | 468.9 | [48] |
| 5 | NiAl LDH@Ni foam | 0–0.5 | 397.5 | [49] |
| 6 | MnCo LDH | 0–0.5 | 229.95 | [50] |
| 7 | $MnNi(OH)_2$ LDH | 0–1 | 160 | [51] |
| 8 | ZnNiCo LDH | 0–0.6 | 183 | [52] |
| 9 | CoAl LDH/GO | −0.1–0.55 | 501.8 | [53] |
| 10 | CuCo LDH | 0–0.55 | 433.95 | [54] |
| 11 | Graphene/$Co(OH)_2$ | 0–0.5 | 237 | [55] |
| 12 | NiCoFe LDH | 0.05–0.55 | 912.5 | [56] |
| 13 | CoNiFe LDH | 0.1–0.45 | 344.75 | [57] |
| **14** | **CoNiFe LDH (CNFL)** | **−0.2–0.4** | **360** | **This work** |

resistance between the electrode and the electrolyte, whereas the $R_{ct2}$ denotes the internal grain resistance of the electrode [59]. The $R_e$ includes the electrolyte resistance, internal resistance of the active materials and contact resistance between the electrode material and the substrate [60]. The magnified inset image clearly shows that the ionic resistances of all the electrodes were almost negligible. The contribution of intrinsic and ionic resistances ($R_e$) of CNL, CFL, NFL and CNFL electrodes were estimated as 1.23, 0.99, 1.36 and 1.9 Ω, respectively. $R_{ct1}$ values for CNL, CFL, NFL and CNFL electrodes were calculated as 0.35, 0.27, 0.42 and 0.16 Ω, respectively. $R_{ct2}$ values of CNL, CFL, NFL and CNFL electrodes were found to be 16.1, 34.67, 470.7 and 11.64 Ω, respectively. The value of $R_{ct1}$ for the CNFL electrode found to be lower than $R_{ct2}$, implying the efficient electron transport between the electrode and the electrolyte [59]. Also, the CNFL electrode exhibited the lower value of $R_{ct2}$, signifying ingenious electronic transport in the electrodes. Vertical spikes in the lower frequency region represent the Warburg impedance which is related to the ionic diffusion in the electrolyte [61]. In the case of the CNFL electrode, an ambiguous semicircle in the higher frequency followed by a vertical spike in the lower frequency infers a rapid charge transfer process which is controlled by the ion diffusion [62]. The lower resistance of ternary CNFL LDH may be attributed to the addition of a third metal ion that not only enhances the electrical conductivity but also intensifies the electrochemical performance of the electrode.

### 3.5. Electro-catalytic study

The OER catalytic activity of prepared LDHs was analyzed by recording the iR compensated LSV curves (Fig. 5A). The overpotential required to achieve the current density of 10 mA $cm^{-2}$ for thin film catalysts CNL, CFL, NFL and CNFL was estimated as 217, 212, 258 and

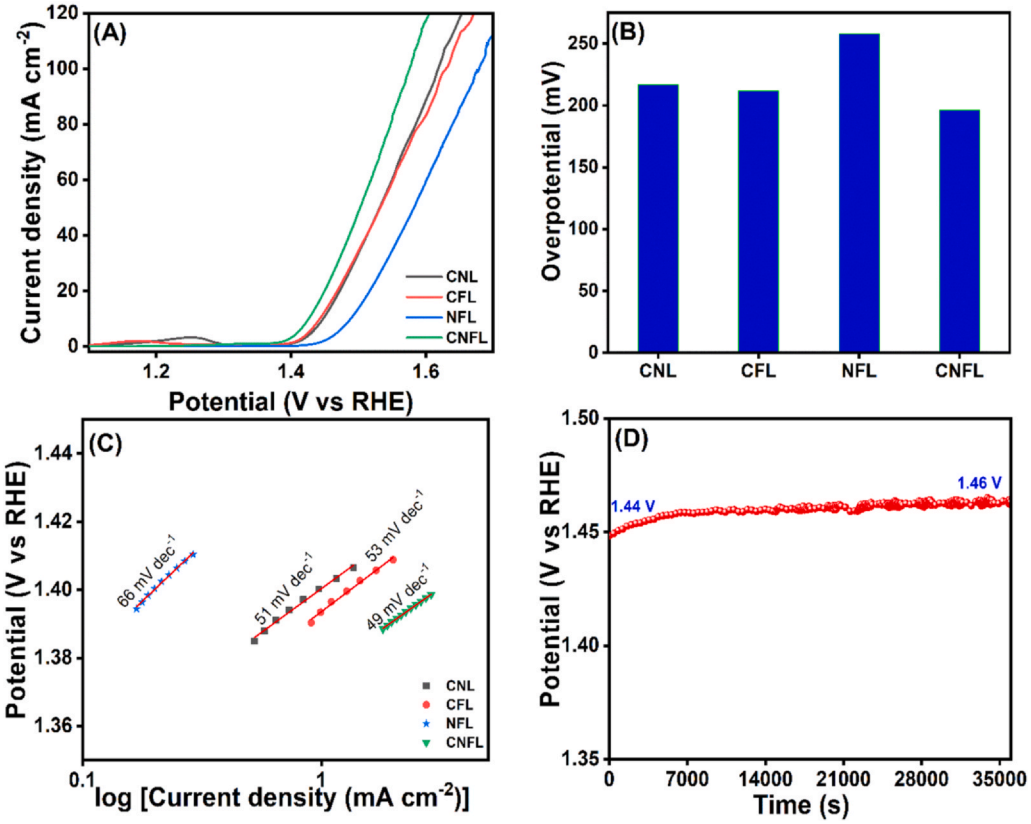


**Fig. 5.** (A) iR compensated LSV curves of CNL, CFL, NFL and CNFL electrodes at the scan rate of 5 mV $s^{-1}$, (B) histogram of overpotentials of different catalysts achieved to attain the current density of 10 mA $cm^{-2}$, (C) Tafel plots obtained from the LSV data and (D) chronopotentiometric curve of CNFL at the constant current density of 10 mA $cm^{-2}$ for 10 h.

196 mV, respectively (Fig. 5B). The histogram shows that the ternary CoNiFe LDH is the best OER catalyst among the other binary LDHs. The improved catalytic activity of ternary LDH is attributed to the synergic effect of Co, Ni and Fe elements in the LDH. Besides, the open and nanostructured morphology of ternary LDH with the high surface area could enable an ample amount of electroactive sites for electrocatalytic reactions [63]. Furthermore, the Tafel slopes of CNL, CFL, NFL and CNFL catalysts were estimated as 51, 53, 66 and 49 mV $dec^{-1}$, respectively (Fig. 5C). The Tafel slope of ternary CoNiFe LDH is the lowest as compared to other binary LDHs, indicating the capability of ternary LDH as a potential electrocatalyst for OER activity. As shown in Fig. 5D, the stability of the CNFL catalyst was studied using chronopotentiometry at the constant current density of 10 mA $cm^{-2}$ for 10 h. The potential was increased from 1.44 to 1.46 V after 10 h which demonstrates that the ternary CoNiFe LDH is a promising electrocatalyst for OER activity. The catalytic activity of the ternary LDH is far better than that of the LDHs reported previously in the literature (Table S2).

## 4. Conclusion

In summary, Co, Ni and Fe based binary and ternary LDHs were successfully prepared via facile electrodeposition method and their electrochemical performances were compared. This study concludes that the ternary CoNiFe LDH exhibits better electrochemical performance for both supercapacitor and OER catalytic applications as compared to binary CoNi, CoFe and NiFe LDHs. The ternary CoNiFe LDH shows a maximum specific capacity of 360 C $g^{-1}$ at the current density of 0.4 A $g^{-1}$ with a capacity retention of 51% even at the higher current density of 10 A $g^{-1}$. It also exhibits excellent stability of 81.4% after 2000 GCD cycles. In the case of electrocatalytic study, ternary CoNiFe LDH requires a minimum overpotential of 196 mV to reach the current density of 10 mA $cm^{-2}$ with Tafel slope value of 49 mV $dec^{-1}$. The CNFL shows the excellent catalytic stability with a very small increment in the overpotential (1.44–1.46 V) after 10 h. Thus, the electrodeposited ternary CoNiFe LDH is a promising electrode material as compared to the binary LDHs for both supercapacitor and electrocatalytic applications.

## CRediT authorship contribution statement

**R.C. Rohit:** Data curation, Writing - original draft, preparation, Software, Investigation. **Ajay D. Jagadale:** Resources, Conceptualization, Methodology, Writing - review & editing, Supervision. **S.K. Shinde:** Resources, Review, Supervision. **D.-Y. Kim:** Review, Supervision. **Vijay S. Kumbhar:** Validation, Review. **Masaharu Nakayama:** Resources, Review, Supervision.

## Declaration of Competing Interest

The authors declare that they have no known competing financial interests or personal relationships that could have appeared to influence the work reported in this paper.

## Acknowledgments

ADJ is thankful to the Department of Science and Technology (DST), Govt. of India for financial assistance under the DST INSPIRE Faculty Scheme [DST/INSPIRE/04/2017/002737].

## Appendix A. Supplementary material

Supplementary data associated with this article can be found in the online version at doi:10.1016/j.jallcom.2020.158081.

## References

[1] Poonam K. Sharma, A. Arora, S.K. Tripathi, Review of supercapacitors: materials and devices, J. Energy Storage 21 (2019) 801–825, https://doi.org/10.1016/j.est.2019.01.010.
[2] L. Liu, H. Zhang, Y. Mu, Y. Bai, Y. Wang, Binary cobalt ferrite nanomesh arrays as the advanced binder-free electrode for applications in oxygen evolution reaction and supercapacitors, J. Power Sources 327 (2016) 599–609, https://doi.org/10.1016/j.jpowsour.2016.07.104.
[3] M.S. Javed, S.S.A. Shah, S. Hussain, S. Tan, W. Mai, Mesoporous manganese-selenide microflowers with enhanced electrochemical performance as a flexible symmetric 1.8 V supercapacitor, Chem. Eng. J. 382 (2020) 122814, https://doi.org/10.1016/j.cej.2019.122814.
[4] K. Li, X. Liu, T. Zheng, D. Jiang, Z. Zhou, C. Liu, X. Zhang, Y. Zhang, D. Losic, Tuning MnO2 to FeOOH replicas with bio-template 3D morphology as electrodes for high performance asymmetric supercapacitors, Chem. Eng. J. 370 (2019) 136–147, https://doi.org/10.1016/j.cej.2019.03.190.
[5] W. Hu, H. Wei, Y. She, X. Tang, M. Zhou, Z. Zang, J. Du, C. Gao, Y. Guo, D. Bao, Flower-like nickel-zinc-cobalt mixed metal oxide nanowire arrays for electrochemical capacitor applications, J. Alloy. Compd. 708 (2017) 146–153, https://doi.org/10.1016/j.jallcom.2017.02.301.
[6] G. Wang, L. Zhang, J. Zhang, A review of electrode materials for electrochemical supercapacitors, Chem. Soc. Rev. 41 (2012) 797–828, https://doi.org/10.1039/C1CS15060J.
[7] J.M. Gonçalves, P.R. Martins, L. Angnes, K. Araki, Recent advances in ternary layered double hydroxide electrocatalysts for the oxygen evolution reaction, New J. Chem. 44 (2020) 9981–9997, https://doi.org/10.1039/D0NJ00021C.
[8] Q. Qian, Y. Li, Y. Liu, G. Zhang, General anion-exchange reaction derived amorphous mixed-metal oxides hollow nanoprisms for highly efficient water oxidation electrocatalysis, Appl. Catal. B Environ. 266 (2020) 118642, https://doi.org/10.1016/j.apcatb.2020.118642.
[9] J. Zhao, J. Chen, S. Xu, M. Shao, Q. Zhang, F. Wei, J. Ma, M. Wei, D.G. Evans, X. Duan, Hierarchical NiMn layered double hydroxide/carbon nanotubes architecture with superb energy density for flexible supercapacitors, Adv. Funct. Mater. 24 (2014) 2938–2946, https://doi.org/10.1002/adfm.201303638.
[10] G. Chen, H. Wan, W. Ma, N. Zhang, Y. Cao, X. Liu, J. Wang, R. Ma, Layered metal hydroxides and their derivatives: controllable synthesis, chemical exfoliation, and electrocatalytic applications, Adv. Energy Mater. 10 (2020) 1902535, https://doi.org/10.1002/aenm.201902535.
[11] S. Moolayadukkam, S. Thomas, R.C. Sahoo, C.H. Lee, S.U. Lee, H.S.S.R. Matte, Role of transition metals in layered double hydroxides for differentiating the oxygen evolution and nonenzymatic glucose sensing, ACS Appl. Mater. Interfaces 12 (2020) 6193–6204, https://doi.org/10.1021/acsami.9b18186.
[12] A.D. Jagadale, G. Guan, X. Li, X. Du, X. Ma, X. Hao, A. Abudula, Ultrathin nanoflakes of cobalt–manganese layered double hydroxide with high reversibility for asymmetric supercapacitor, J. Power Sources 306 (2016) 526–534, https://doi.org/10.1016/j.jpowsour.2015.12.097.
[13] H. Chen, L. Hu, M. Chen, Y. Yan, L. Wu, Nickel–cobalt layered double hydroxide nanosheets for high-performance supercapacitor electrode materials, Adv. Funct. Mater. 24 (2014) 934–942, https://doi.org/10.1002/adfm.201301747.
[14] L. Wang, D. Wang, X.Y. Dong, Z.J. Zhang, X.F. Pei, X.J. Chen, B. Chen, J. Jin, Layered assembly of graphene oxide and Co–Al layered double hydroxide nanosheets as electrode materials for supercapacitors, Chem. Commun. 47 (2011) 3556–3558, https://doi.org/10.1039/C0CC05420H.
[15] Y. Wimalasiri, R. Fan, X.S. Zhao, L. Zou, Assembly of Ni-Al layered double hydroxide and graphene electrodes for supercapacitors, Electrochim. Acta 134 (2014) 127–135, https://doi.org/10.1016/j.electacta.2014.04.129.
[16] X.L. Guo, X.Y. Liu, X.D. Hao, S.J. Zhu, F. Dong, Z.Q. Wen, Y.X. Zhang, Nickel-manganese layered double hydroxide nanosheets supported on nickel foam for high-performance supercapacitor electrode materials, Electrochim. Acta 194 (2016) 179–186, https://doi.org/10.1016/j.electacta.2016.02.080.
[17] X. Gao, X. Liu, D. Wu, B. Qian, Z. Kou, Z. Pan, Y. Pang, L. Miao, J. Wang, Significant role of Al in ternary layered double hydroxides for enhancing electrochemical performance of flexible asymmetric supercapacitor, Adv. Funct. Mater. 29 (2019) 1903879, https://doi.org/10.1002/adfm.201903879.
[18] P. Li, X. Duan, Y. Kuang, Y. Li, G. Zhang, W. Liu, X. Sun, Tuning electronic structure of NiFe layered double hydroxides with vanadium doping toward high efficient electrocatalytic water oxidation, Adv. Energy Mater. 8 (2018) 1703341, https://doi.org/10.1002/aenm.201703341.
[19] Y. Zeng, M. Yu, Y. Meng, P. Fang, X. Lu, Y. Tong, Iron-based supercapacitor electrodes: advances and challenges, Adv. Energy Mater. 6 (2016) 1601053, https://doi.org/10.1002/aenm.201601053.
[20] K. Li, S. Feng, C. Jing, Y. Chen, X. Liu, Y. Zhang, L. Zhou, Assembling a double shell on a diatomite skeleton ternary complex with conductive polypyrrole for the enhancement of supercapacitors, Chem. Commun. 55 (2019) 13773–13776, https://doi.org/10.1039/C9CC06791D.
[21] F. Wang, S. Sun, Y. Xu, T. Wang, R. Yu, H. Li, High performance asymmetric supercapacitor based on cobalt nickle iron-layered double hydroxide/carbon nanofibres and activated carbon, Sci. Rep. 7 (2017) 4707, https://doi.org/10.1038/s41598-017-04807-1.
[22] N.L.W. Septiani, Y.V. Kaneti, Y. Guo, B. Yuliarto, X. Jiang, Y. Ide, N. Nugraha, H.K. Dipojono, A. Yu, Y. Sugahara, D. Golberg, Y. Yamauchi, Holey assembly of two-dimensional iron-doped nickel-cobalt layered double hydroxide nanosheets for energy conversion application, ChemSusChem 13 (2020) 1645–1655, https://doi.org/10.1002/cssc.201901364.

[23] C. Dong, L. Han, C. Zhang, Z. Zhang, Scalable dealloying route to mesoporous ternary CoNiFe layered double hydroxides for efficient oxygen evolution, ACS Sustain. Chem. Eng. 6 (2018) 16096–16104, https://doi.org/10.1021/acssuschemeng.8b02656.
[24] F. Li, Z. Sun, H. Jiang, Z. Ma, Q. Wang, F. Qu, Ion-exchange synthesis of ternary FeCoNi layered double hydroxide nanocage towards enhanced oxygen evolution reaction and supercapacitor, Energy Fuels (2020), https://doi.org/10.1021/acs.energyfuels.0c02533.
[25] B. Pandit, D.P. Dubal, B.R. Sankapal, Large scale flexible solid state symmetric supercapacitor through inexpensive solution processed V2O5 complex surface architecture, Electrochim. Acta 242 (2017) 382–389, https://doi.org/10.1016/j.electacta.2017.05.010.
[26] R.C. Rohit, A. Jenifer, A.D. Jagadale, V.S. Kumbhar, H. Lee, K. Lee, Facile synthesis of Ce-doped α-cobalt hydroxide nanoflakes battery type electrode with an enhanced capacitive contribution for asymmetric supercapacitors, J. Energy Storage 28 (2020) 101227, https://doi.org/10.1016/j.est.2020.101227.
[27] M. Shao, R. Zhang, Z. Li, M. Wei, D.G. Evans, X. Duan, Layered double hydroxides toward electrochemical energy storage and conversion: design, synthesis and applications, Chem. Commun. 51 (2015) 15880–15893, https://doi.org/10.1039/C5CC07296D.
[28] L. Jiang, Y. Sui, J. Qi, Y. Chang, Y. He, Q. Meng, F. Wei, Z. Sun, Y. Jin, Structure dependence of Fe-Co hydroxides on Fe/Co ratio and their application for supercapacitors, Part. Part. Syst. Charact. 34 (2017) 1600239, https://doi.org/10.1002/ppsc.201600239.
[29] B. Li, P. Gu, Y. Feng, G. Zhang, K. Huang, H. Xue, H. Pang, Ultrathin nickel–cobalt phosphate 2D nanosheets for electrochemical energy storage under aqueous/solid-state electrolyte, Adv. Funct. Mater. 27 (2017) 1605784, https://doi.org/10.1002/adfm.201605784.
[30] Z. Gholamvand, D. McAteer, A. Harvey, C. Backes, J.N. Coleman, Electrochemical applications of two-dimensional nanosheets: the effect of nanosheet length and thickness, Chem. Mater. 28 (2016) 2641–2651, https://doi.org/10.1021/acs.chemmater.6b00009.
[31] X. Zheng, Z. Gu, Q. Hu, B. Geng, X. Zhang, Ultrathin porous nickel–cobalt hydroxide nanosheets for high-performance supercapacitor electrodes, RSC Adv. 5 (2015) 17007–17013, https://doi.org/10.1039/C5RA01294E.
[32] S. Luo, L. Qian, M. Liao, X. Hu, D. Xiao, Surface and interface engineering of CoNi layered double hydroxides for efficient methanol oxidation reaction, RSC Adv. 7 (2017) 45294–45303, https://doi.org/10.1039/C7RA07867F.
[33] D. Pan, S. Ge, J. Zhao, Q. Shao, L. Guo, X. Zhang, J. Lin, G. Xu, Z. Guo, Synthesis, characterization and photocatalytic activity of mixed-metal oxides derived from NiCoFe ternary layered double hydroxides, Dalton Trans. 47 (2018) 9765–9778, https://doi.org/10.1039/C8DT01045E.
[34] M. Arif, G. Yasin, M. Shakeel, M. Asim Mushtaq, W. Ye, X. Fang, S. Ji, D. Yan, Hierarchical CoFe-layered double hydroxide and g-C3N4 heterostructures with enhanced bifunctional photo/electrocatalytic activity towards overall water splitting, Mater. Chem. Front. 3 (2019) 520–531, https://doi.org/10.1039/C8QM00677F.
[35] L. Liu, X. Hu, H.-Y. Zeng, M.-Y. Yi, S.-G. Shen, S. Xu, X. Cao, J.-Z. Du, Preparation of NiCoFe-hydroxide/polyaniline composite for enhanced-performance supercapacitors, J. Mater. Sci. Technol. 35 (2019) 1691–1699, https://doi.org/10.1016/j.jmst.2019.04.003.
[36] X. Ge, C.D. Gu, X.L. Wang, J.P. Tu, Ionothermal synthesis of cobalt iron layered double hydroxides (LDHs) with expanded interlayer spacing as advanced electrochemical materials, J. Mater. Chem. A 2 (2014) 17066–17076, https://doi.org/10.1039/C4TA03789H.
[37] W. Huang, S. Ding, Y. Chen, W. Hao, X. Lai, J. Peng, J. Tu, Y. Cao, X. Li, 3D NiO hollow sphere/reduced graphene oxide composite for high-performance glucose biosensor, Sci. Rep. 7 (2017) 1–11, https://doi.org/10.1038/s41598-017-05528-1.
[38] F.B.D. Saiah, B.-L. Su, N. Bettahar, Nickel–iron layered double hydroxide (LDH): textural properties upon hydrothermal treatments and application on dye sorption, J. Hazard. Mater. 165 (2009) 206–217, https://doi.org/10.1016/j.jhazmat.2008.09.125.
[39] G.Y. Abo El-Reesh, A.A. Farghali, M. Taha, R.K. Mahmoud, Novel synthesis of Ni/Fe layered double hydroxides using urea and glycerol and their enhanced adsorption behavior for Cr(VI) removal, Sci. Rep. 10 (2020) 587, https://doi.org/10.1038/s41598-020-57519-4.
[40] F.A. Najar, G.B. Vakil, B. Want, Structural, optical and dielectric studies of lithium sulphate monohydrate single crystals, Mater. Sci. 35 (2017) 18–31, https://doi.org/10.1515/msp-2017-0002 Poland.
[41] Y. Tang, Y. Liu, S. Yu, W. Guo, S. Mu, H. Wang, Y. Zhao, L. Hou, Y. Fan, F. Gao, Template-free hydrothermal synthesis of nickel cobalt hydroxide nanoflowers with high performance for asymmetric supercapacitor, Electrochim. Acta 161 (2015) 279–289, https://doi.org/10.1016/j.electacta.2015.02.095.
[42] Y. Zhu, S. An, X. Sun, D. Lan, J. Cui, Y. Zhang, W. He, Core-branched NiCo2S4@CoNi-LDH heterostructure as advanced electrode with superior energy storage performance, Chem. Eng. J. 383 (2020) 123206, https://doi.org/10.1016/j.cej.2019.123206.
[43] C. Tang, H.-S. Wang, H.-F. Wang, Q. Zhang, G.-L. Tian, J.-Q. Nie, F. Wei, Spatially confined hybridization of nanometer-sized NiFe hydroxides into nitrogen-doped graphene frameworks leading to superior oxygen evolution reactivity, Adv. Mater. 27 (2015) 4516–4522, https://doi.org/10.1002/adma.201501901.
[44] B. Shruthi, B.J. Madhu, V.B. Raju, S. Vynatheya, B.V. Devi, G.V. Jayashree, C.R. Ravikumar, Synthesis, Spectroscopic Analysis and Electrochemical Performance of Modified β-nickel Hydroxide Electrode with CuO, 2017. ⟨http://repository.ntt.edu.vn/jspui/handle/298300331/2274⟩ (Accessed 27 September 2020).
[45] D.S. Hall, D.J. Lockwood, S. Poirier, C. Bock, B.R. MacDougall, Raman and infrared spectroscopy of α and β phases of thin nickel hydroxide films electrochemically formed on nickel, J. Phys. Chem. A 116 (2012) 6771–6784, https://doi.org/10.1021/jp303546r.
[46] Y.-L. Liu, C. Yan, G.-G. Wang, H.-Y. Zhang, L.-Y. Dang, B.-W. Wu, Z.-Q. Lin, X.-S. An, J.-C. Han, Achieving ultrahigh capacity with self-assembled Ni(OH)2 nanosheet-decorated hierarchical flower-like MnCo2O4.5 nanoneedles as advanced electrodes of battery–supercapacitor hybrid devices, ACS Appl. Mater. Interfaces 11 (2019) 9984–9993, https://doi.org/10.1021/acsami.8b21803.
[47] J. Xu, S. Gai, F. He, N. Niu, P. Gao, Y. Chen, P. Yang, Reduced graphene oxide/Ni1−xCoxAl-layered double hydroxide composites: preparation and high supercapacitor performance, Dalton Trans. 43 (2014) 11667–11675, https://doi.org/10.1039/C4DT00686K.
[48] Z. Gao, J. Wang, Z. Li, W. Yang, B. Wang, M. Hou, Y. He, Q. Liu, T. Mann, P. Yang, M. Zhang, L. Liu, Graphene nanosheet/Ni2+/Al3+ layered double-hydroxide composite as a novel electrode for a supercapacitor, Chem. Mater. 23 (2011) 3509–3516, https://doi.org/10.1021/cm200975x.
[49] B. Wang, Q. Liu, Z. Qian, X. Zhang, J. Wang, Z. Li, H. Yan, Z. Gao, F. Zhao, L. Liu, Two steps in situ structure fabrication of Ni–Al layered double hydroxide on Ni foam and its electrochemical performance for supercapacitors, J. Power Sources 246 (2014) 747–753, https://doi.org/10.1016/j.jpowsour.2013.08.035.
[50] N. Wu, J. Low, T. Liu, J. Yu, S. Cao, Hierarchical hollow cages of Mn-Co layered double hydroxide as supercapacitor electrode materials, Appl. Surf. Sci. 413 (2017) 35–40, https://doi.org/10.1016/j.apsusc.2017.03.297.
[51] S. Anandan, C.-Y. Chen, J.J. Wu, Sonochemical synthesis and characterization of turbostratic MnNi(OH)2 layered double hydroxide nanoparticles for supercapacitor applications, RSC Adv. 4 (2014) 55519–55523, https://doi.org/10.1039/C4RA10816G.
[52] Z.-H. Huang, F.-F. Sun, M. Batmunkh, W.-H. Li, H. Li, Y. Sun, Q. Zhao, X. Liu, T.-Y. Ma, Zinc–nickel–cobalt ternary hydroxide nanoarrays for high-performance supercapacitors, J. Mater. Chem. A. 7 (2019) 11826–11835 https://doi.org/10.1039/C9TA01995B.
[53] J. Fang, M. Li, Q. Li, W. Zhang, Q. Shou, F. Liu, X. Zhang, J. Cheng, Microwave-assisted synthesis of CoAl-layered double hydroxide/graphene oxide composite and its application in supercapacitors, Electrochim. Acta 85 (2012) 248–255, https://doi.org/10.1016/j.electacta.2012.08.078.
[54] S. Liu, K.S. Hui, K.N. Hui, V.V. Jadhav, Q.X. Xia, J.M. Yun, Y.R. Cho, R.S. Mane, K.H. Kim, Facile synthesis of microsphere copper cobalt carbonate hydroxides electrode for asymmetric supercapacitor, Electrochim. Acta 188 (2016) 898–908, https://doi.org/10.1016/j.electacta.2015.12.018.
[55] Z. Li, J. Wang, L. Niu, J. Sun, P. Gong, W. Hong, L. Ma, S. Yang, Rapid synthesis of graphene/cobalt hydroxide composite with enhanced electrochemical performance for supercapacitors, J. Power Sources 245 (2014) 224–231, https://doi.org/10.1016/j.jpowsour.2013.06.121.
[56] H. Li, Y. Gao, C. Wang, G. Yang, A simple electrochemical route to access amorphous mixed-metal hydroxides for supercapacitor electrode materials, Adv. Energy Mater. 5 (2015) 1401767, https://doi.org/10.1002/aenm.201401767.
[57] L. Su, Z. Song, J. Guo, J. Li, Synthesis and low-temperature capacitive performances of ternary active site CoNiFe hydroxides, ChemistrySelect 2 (2017) 2665–2669, https://doi.org/10.1002/slct.201700071.
[58] J.M. Gonçalves, P.R. Martins, K. Araki, L. Angnes, Recent progress in water splitting and hybrid supercapacitors based on nickel-vanadium layered double hydroxides, J. Energy Chem. (2020), https://doi.org/10.1016/j.jechem.2020.08.047.
[59] K. Ashok Kumar, A. Pandurangan, S. Arumugam, M. Sathiskumar, Effect of bifunctional hierarchical flower-like CoS nanostructure on its interfacial charge transport kinetics, magnetic and electrochemical behaviors for supercapacitor and DSSC applications, Sci. Rep. 9 (2019) 1228, https://doi.org/10.1038/s41598-018-37463-0.
[60] M. Li, R. Jijie, A. Barras, P. Roussel, S. Szunerits, R. Boukherroub, NiFe layered double hydroxide electrodeposited on Ni foam coated with reduced graphene oxide for high-performance supercapacitors, Electrochim. Acta 302 (2019) 1–9, https://doi.org/10.1016/j.electacta.2019.01.187.
[61] Y. Liu, N. Fu, G. Zhang, M. Xu, W. Lu, L. Zhou, H. Huang, Design of hierarchical Ni–Co@Ni–Co layered double hydroxide core-shell structured nanotube array for high-performance flexible all-solid-state battery-type supercapacitors, Adv. Funct. Mater. 27 (2017) 1605307, https://doi.org/10.1002/adfm.201605307.
[62] Y. Wang, S. Dong, X. Wu, M. Li, One-step electrodeposition of MnO2@NiAl layered double hydroxide nanostructures on the nickel foam for high-performance supercapacitors, J. Electrochem. Soc. 164 (2016) H56–H62, https://doi.org/10.1149/2.0861702jes.
[63] L. Yu, J.F. Yang, B.Y. Guan, Y. Lu, X.W. (David) Lou, Hierarchical hollow nanoprisms based on ultrathin Ni-Fe layered double hydroxide nanosheets with enhanced electrocatalytic activity towards oxygen evolution, Angew. Chem. Int. Ed. 57 (2018) 172–176, https://doi.org/10.1002/anie.201710877.